JOURNAL OF CATALYSIS **164,** 1–15 (1996)
ARTICLE NO. 0357

MgO-Supported Platinum–Tungsten Catalysts Prepared from Organometallic Precursors: Platinum Clusters Isolated on Dispersed Tungsten

O. Alexeev,* M. Shelef,† and B. C. Gates*

*Department of Chemical Engineering and Materials Science, University of California, Davis, California 95616; and †Scientific Research Staff, Ford Motor Co., Dearborn, Michigan 48121

Received December 18, 1995; revised June 28, 1996; accepted July 16, 1996

MgO-supported Pt and Pt–W catalysts were prepared from organometallic precursors and characterized to determine how the nature of the precursors and the treatment conditions affected the Pt–W interactions and the catalytic activity for toluene hydrogenation. Samples were prepared from $\{Pt[W(CO)_3(C_5H_5)]_2(PhCN)_2\}$ (Ph = phenyl) and from $[PtCl_2(PhCN)_2] + [W(CO)_6]$ and characterized by infrared spectroscopy, extended X-ray absorption fine structure (EXAFS) spectroscopy, transmission electron microscopy (TEM), and chemisorption of H_2, CO, and O_2. The samples were treated in H_2 at 400°C prior to most of the characterizations. Incorporation of W reduced the chemisorption of CO and of H_2, with the reduction in chemisorption being greater for the catalyst prepared from $\{Pt[W(CO)_3(C_5H_5)]_2(PhCN)_2\}$ than for the catalyst prepared from the combination of monometallic precursors. EXAFS spectra measured at both the Pt L_{II} edge and the W L_{III} edge showed substantial Pt–W contributions for the former catalyst (but not the latter), with a Pt–W coordination number of about 2 and an average Pt–W distance of 2.71 Å. TEM and EXAFS results indicate that interactions between Pt and W cations in the sample made from $\{Pt[W(CO)_3(C_5H_5)]_2(PhCN)_2\}$ maintained the Pt in a highly dispersed form, with supported Pt clusters being smaller than about 10 Å. The catalyst prepared from the bimetallic cluster was more than an order of magnitude less active for toluene hydrogenation at 1 atm and 60°C than the catalyst prepared from the two monometallic precursors; the comparison indicates that the W acted like an isolated dispersed support, with its influence on the catalysis maximized by its proximity to the Pt.

INTRODUCTION

Supported bimetallic catalysts are used in large-scale applications, as illustrated by catalysts containing Pt and Re for naphtha reforming (1) and catalysts containing Pt and Rh for simultaneous removal of CO, hydrocarbons, and NO from automobile exhaust (2–9). Some bimetallic structures are alloy-like (10), but others incorporate segregated metals, sometimes with one of the metals in a cationic form, perhaps as a metal oxide (11, 12). Most conventional preparations of supported bimetallic particles involve coprecipitation or coimpregnation followed by a high-temperature reduction giving structurally nonuniform materials with relatively large metal particles. It is difficult to characterize the structure and nature of the bimetallic interactions in these materials.

Organometallic chemistry has been used to prepare supported catalysts with well-defined and/or highly dispersed bimetallic structures. For example, catalysts were prepared by formation of highly dispersed particles of a noble metal followed by addition of a complex of an oxophilic metal (11, 13). Bimetallic precursors have been used to prepare supported bimetallic catalysts with close proximity of the two metals (14, 15), but when one metal is resistant to oxidation and the other is oxophilic, the two typically segregate on the support following removal of the precursor ligands (16). Bimetallic clusters were used to prepare Rh–Mo (17, 18), Fe–*M* (*M* = Os, Ru, Co) (19), Pd–Mo (20), and Pt–Mo (21) catalysts, among others.

We envision catalysts made from bimetallic precursors so that clusters of a noble metal are isolated in association with dispersed structures of an oxophilic metal on the support (20, 21). The oxophilic metal would act like a localized support. The goal of this work was to prepare and characterize supported Pt catalysts starting from $\{Pt[W(CO)_3(C_5H_5)]_2(PhCN)_2\}$, a precursor in which the Pt and W are initially bonded to each other; the intent was to prepare supported samples in which isolated clusters of Pt atoms are linked to small tungsten oxide-like structures on the support. MgO was chosen as the support because it stabilizes adsorbed metal carbonyl clusters (22) and was expected to allow adsorption of $\{Pt[W(CO)_3(C_5H_5)]_2(PhCN)_2\}$ intact or nearly intact. For comparison, samples were made by coadsorption of $[PtCl_2(PhCN)_2]$ and $[W(CO)_6]$.

EXPERIMENTAL METHODS

Materials and sample preparation. $\{Pt[W(CO)_3 \cdot (C_5H_5)]_2(PhCN)_2\}$ was used to prepare the sample denoted $(PtW_2)/MgO$. $\{Pt[W(CO)_3(C_5H_5)]_2(PhCN)_2\}$ was

0021-9517/96 $18.00

synthesized from $[PtCl_2(PhCN)_2]$ and $Na[W(CO)_3Cp]\cdot 2DME$ (DME is 1,2-dimethoxyethane) in tetrahydrofuran solution at $-40^\circ C$ under N_2. After purification, the product was isolated as a orange powder. The ν_{CO} infrared spectrum agrees with previous observations (23, 24). $[PtCl_2(PhCN)_2]$ and $[W(CO)_6]$ (Strem) were used without purification to prepare the sample referred to as (Pt + W)/MgO.

The MgO support (MX-65-1 powder, MCB reagents), with a BET surface area of 47 m^2/g, was calcined in flowing O_2 at 400°C for 2 h, followed by evacuation (10^{-3} Torr) at 400°C for 14 h. *n*-Pentane solvent was distilled over Na/benzophenone and deoxygenated by purging with N_2. (PtW_2)/MgO, (Pt + W)/MgO, and W/MgO were prepared by slurrying of $\{Pt[W(CO)_3(C_5H_5)]_2(PhCN)_2\}$, the mixture of $[PtCl_2(PhCN)_2]$ and $[W(CO)_6]$, and $[W(CO)_6]$ respectively, with MgO powder in freshly distilled pentane under N_2. Each mixture was stirred for 12 h at room temperature followed by solvent removal and evacuation at 25°C overnight. The synthesis and handling were carried out with standard air exclusion techniques by use of a Schlenk vacuum line and a N_2-filled drybox. Samples contained 2 wt% W and 1 wt% Pt (if any). Before characterization, each sample was reduced with H_2 at 1 atm and 400°C.

Transmission electron microscopy (TEM). Samples were characterized with a Zeiss Electron Microscope, EM-109. The statistical method used to determine the particle mean surface size was similar to that reported elsewhere (25); the mean surface sizes were determined with an accuracy of about ±15%.

Infrared spectroscopy. Infrared experiments were carried out with a Bruker IFS-66v spectrometer. Spectra were recorded at 25°C with a 4-cm^{-1} resolution and averaging of 64 scans. Details of the sample handling are reported elsewhere (21).

Chemisorption. Chemisorption measurements were performed with an RXM-100 multifunctional catalyst testing and characterization instrument manufactured by Advanced Scientific Designs, Inc. (ASDI) with a vacuum capability of 10^{-8} Torr. Each sample in the drybox was loaded into a U-shaped quartz tube, which was closed to prevent contamination of the sample as it was transferred to the chemisorption apparatus. Before chemisorption measurements, each sample was treated in flowing H_2 as the temperature was ramped at 5°C/min and held at the final temperature for 2 h. It was then evacuated (10^{-7} Torr) and cooled to room temperature. Adsorption isotherms were measured at 25°C and 10–200 Torr. The amount of hydrogen, CO, or oxygen irreversibly chemisorbed on each sample was measured as the difference between two consecutively measured isotherms (the total adsorption and the physical adsorption) with 30 minutes' evacuation between measurements. Accuracy in the determination of H/*M*, CO/*M*, and O/*M* (where *M* is metal) values was about ±1%.

Catalytic testing. Toluene hydrogenation was carried out at atmospheric pressure in a Pyrex flow reactor at 60°C. The H_2 was purified by flow through activated traps containing zeolite 4A and Cu. Prior to reaction, the samples were reduced in H_2 as the temperature was ramped to 400°C at 5°C/min and then held at 400°C for 2 h. Toluene was fed by an Isco syringe pump to a vaporization chamber, where it was mixed with H_2. The toluene and H_2 flow rates were adjusted to give partial pressures of 50 and 710 Torr, respectively. The products were analyzed with an on-line gas chromatograph equipped with a flame ionization detector. In the absence of catalyst, there was no measurable conversion of toluene. Accuracy in the determination of reaction rates was about ±10%.

Extended X-ray absorption fine structure (EXAFS) spectroscopy. EXAFS experiments were performed on X-ray beamline X-11A at the National Synchrotron Light Source at Brookhaven National Laboratory, Upton, New York. The ring energy was 2.5 GeV; the ring current was 80–220 mA. Spectra were recorded with the sample in a cell that allowed treatment in flowing gases prior to the measurements.

Both (PtW_2)/MgO and (Pt + W)/MgO were characterized by EXAFS spectroscopy. The EXAFS spectra were acquired after treatment of each sample in H_2 at 400°C, O_2 at 200 or 400°C, and then H_2 at 400°C. Each powder sample was pressed into a wafer with a C-clamp in a glovebox. The mass of sample was chosen to give an absorbance of about 2.5 at the Pt L_{II} and W L_{III} absorption edges. After the sample had been pressed, it was loaded into an EXAFS cell, sealed under positive N_2 pressure, and removed from the drybox. The sample was treated in flowing purified H_2 at 400°C for 2 h, cooled to room temperature in flowing H_2, evacuated to 10^{-5} Torr, and aligned in the X-ray beam.

The EXAFS data were recorded in the transmission mode after the cell had been cooled to nearly liquid nitrogen temperature. The data were collected with a Si(111) double crystal monochromator that was detuned by 20% to minimize the effects of higher harmonics in the X-ray beam. The samples were scanned at energies near the Pt L_{II} edge (13272.6 eV) and the W L_{II} edge (10206.8 eV).

EXAFS reference data. The EXAFS data were analyzed with experimentally and theoretically determined reference files, the former obtained from EXAFS data for materials of known structure. The Pt–Pt, Pt–$O_{support}$, W–W, and W–$O_{support}$ interactions were analyzed with phase shifts and backscattering amplitudes obtained from EXAFS data for Pt foil, $Na_2Pt(OH)_6$, W foil, and K_2WO_4, respectively. The Pt–W and W–Pt interactions were calculated by using the FEFF software (26). The parameters used to extract these results from the EXAFS data are summarized in Table 1.

EXAFS data analysis. Because of the overlap of the Pt L_{III} edge (11563.7 eV) with the W L_{II} edge (11544 eV),

TABLE 1

Crystallographic Data Characterizing the Reference Compounds and Fourier Transform Ranges Used in the EXAFS Data Analysis[a]

Sample	FEFF calculation	Crystallographic data			Fourier transform		
		Shell	N	R (Å)	Δk (Å^{-1})	Δr (Å)	n
Pt foil		Pt–Pt	12	2.77	3.65–11.99	1.74–3.49	3
$Na_2Pt(OH)_6$		Pt–O	6	2.05	2.38–11.90	0.43–2.99	3
W foil		W–W	8	2.73	4.00–17.61	0.86–7.97	3
K_2WO_4		W–O	4	1.76	3.73–15.60	0.45–2.18	1
—	PtW	Pt–W	12	2.72	3.53–19.55	1.85–3.07	3
—	WPt	W–Pt	12	2.72	2.84–19.55	1.85–3.07	3

[a] Notation: N, coordination number for absorber–backscatterer pair; R, distance; Δk, limits used for forward Fourier transformation (k is the wave vector); Δr, limits used for shell isolation (r is distance); n, power of k used for Fourier transformation.

the data analysis for the bimetallic sample was done for the W L_{III} (10206.8 eV) and Pt L_{II} (13272.6 eV) edges. The method is limited because the Pt L_{III} edge is close to the Pt L_I (13879.9 eV) edge; the difference of only 607.3 eV between the edges allowed data analysis only up to a value of k, the wave vector, of about 12 Å^{-1}, which is sufficient only for analysis of the first coordination shell.

The EXAFS data were extracted from the spectra with the XDAP software (27, 28). The EXAFS function for each sample was obtained from the X-ray absorption spectrum by a cubic spline background subtraction and normalized by dividing the absorption intensity by the height of the absorption edge. The final normalized EXAFS function for each sample was obtained from the average of six scans. The main contributions to the spectra were isolated by inverse Fourier transformation of the final EXAFS function. The following procedures were applied to the raw EXAFS data.

The raw EXAFS data at the Pt L_{II} edge obtained for (Pt + W)/MgO were Fourier transformed with a k^3 weighting over the range $2.68 < k < 12.23$ Å^{-1} with no phase correction. The Fourier-transformed data were then inverse transformed in the range $0.28 < r < 3.26$ Å (r is the distance from the absorber atom) to isolate the major contributions from low-frequency noise. The EXAFS data analysis was done with 12 free parameters over the range $3.66 < k < 11.7$ Å^{-1} and $0.28 < r < 3.26$ Å. The statistically justified number of free parameters, n, was about 16, as estimated from the Nyquist theorem (29), $n = (2\Delta k \Delta r/\pi) + 1$, where Δk and Δr, respectively, are the k and r ranges used to fit the data.

The raw EXAFS data at the Pt L_{II} edge obtained for (PtW_2)/MgO were Fourier transformed with a k^3 weighting over the range $2.65 < k < 12.16$ Å^{-1} with no phase correction. The Fourier-transformed data were then inverse transformed in the range $0.12 < r < 3.48$ Å to isolate the major contributions from low-frequency noise. The data analysis was done with 16 free parameters over the range $3.66 < k < 11.7$ Å^{-1} and $0.12 < r < 3.48$ Å. The statistically justified number of free parameters, estimated as described above, was about 18.

A similar procedure was used at the W L_{III} edge with the data characterizing (PtW_2)/MgO. The raw data were Fourier transformed with a k^3 weighting over the range $3.5 < k < 15.42$ Å^{-1} with no phase correction. The Fourier-transformed data were then inverse transformed in the range $0.10 < r < 3.42$ Å. The data analysis at the W L_{III} edge was done with 16 free parameters over the range $4.05 < k < 14.0$ Å^{-1} and $0.10 < r < 3.42$ Å. The statistically justified number of free parameters, estimated as described above, was about 22.

With the difference file technique (27, 28), the Pt–Pt contributions in each sample, the largest in the EXAFS spectra, were estimated first and subtracted from the raw data. The difference file was expected to represent Pt–$O_{support}$ as well as Pt–W interactions. After optimizing the parameters for the Pt–$O_{support}$ contributions, the first guess Pt–Pt and Pt–$O_{support}$ contributions were than added and compared with the raw data. The reliable parameters for the high-Z (Pt) and low-Z ($O_{support}$) contributions were determined by multiple-shell fitting in r space and in k space with application of k^1 and k^3 weighting (29, 30). The optimized Pt–Pt and Pt–$O_{support}$ contributions characteristic of (Pt + W)/MgO were subtracted from the raw data. Only noise was present in the difference file, without any evidence of additional high- or low-Z contributions. In contrast, the similarly obtained fit of the Pt L_{II} edge data characterizing (PtW_2)/MgO that included only the sum of the Pt–Pt and Pt–$O_{support}$ contributions was not satisfactory; another contribution, Pt–W, had to be accounted for. A similar analysis was done for the W edge data characterizing (PtW_2)/MgO. These data also indicated a W–Pt interaction; a good fit was obtained only when W–W, W–Pt, and W–$O_{support}$ contributions were included. Because data were obtained at both the Pt L_{II} edge and the W L_{III} edge, it was possible to determine some EXAFS parameters (e.g., the Pt–W distance) from the data at each edge; thus, there

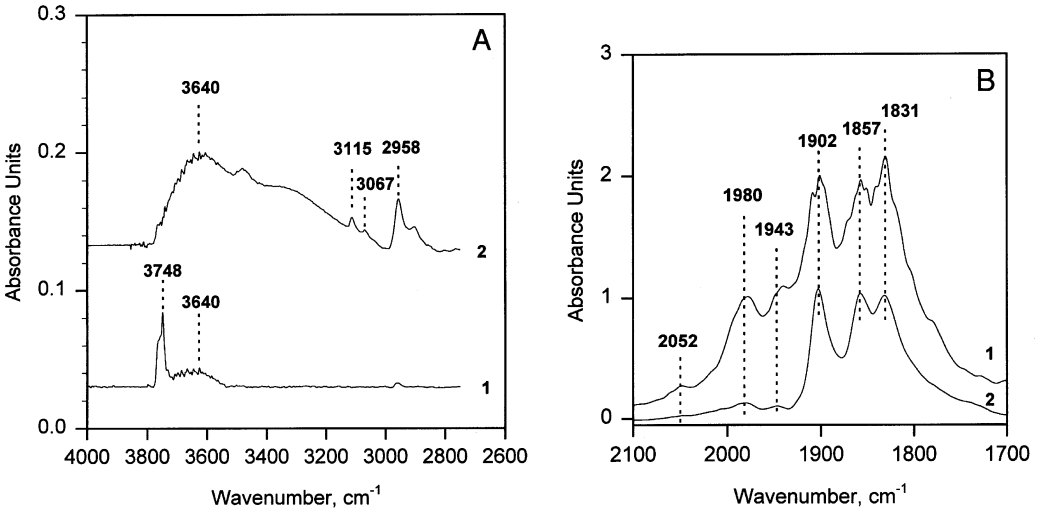

FIG. 1. (A) Infrared spectra in the ν_{OH} and ν_{CH} regions. (1) MgO, recorded after evacuation at 400°C for 14 h; (2) sample formed by contacting of MgO with $\{Pt[W(CO)_3(C_5H_5)]_2(PhCN)_2\}$ in pentane. (B) Infrared spectra in the ν_{CO} region: (1) $\{Pt[W(CO)_3(C_5H_5)]_2(PhCN)_2\}$ mixed with KBr powder; (2) $\{Pt[W(CO)_3(C_5H_5)]_2(PhCN)_2\}$ adsorbed on MgO.

were opportunities to evaluate the internal consistency of the fitting results; the issues are addressed in the Discussion section.

RESULTS

Interaction of $\{Pt[W(CO)_3(C_5H_5)]_2(PhCN)_2\}$ with MgO: Evidence from infrared spectroscopy. The ν_{OH} spectrum of MgO is characterized by a strong band at 3748 cm^{-1}, assigned to surface hydroxyl groups (31, 32) (Fig. 1A, spectrum 1). The weak band at 3640 cm^{-1} indicates traces of hydrogen-bonded hydroxyl groups (31, 32). After slurrying of $\{Pt[W(CO)_3(C_5H_5)]_2(PhCN)_2\}$ with MgO in *n*-pentane followed by evacuation at 25°C, a strong, broad absorption band appeared at 3640 cm^{-1}, associated with the formation of hydrogen-bonded OH groups (31, 32), together with bands at 3115, 3067, and 2958 cm^{-1}, attributed to ν_{CH} in the C_5H_5 and PhCN ligands (33, 34) (Fig. 1A, spectrum 2). *n*-Pentane residues may also have contributed to the ν_{CH} bands in the 2800–3000 cm^{-1} region.

Figure 1B shows ν_{CO} spectra of $\{Pt[W(CO)_3(C_5H_5)]_2 \cdot (PhCN)_2\}$ before and after interaction with MgO. The spectrum of $\{Pt[W(CO)_3(C_5H_5)]_2(PhCN)_2\}$ mixed with KBr powder (Fig. 1B, spectrum 1) is characterized by principal absorption bands at 2052, 1980, 1943, 1902, 1857, and 1831 cm^{-1}, attributed to ν_{CO} (23, 24). After interaction of $\{Pt[W(CO)_3(C_5H_5)]_2(PhCN)_2\}$ with MgO (Fig 1B, spectrum 2), no changes were observed in the carbonyl band positions.

The appearance in the infrared spectrum of intense, overlapping bands at about 1700–1200 cm^{-1} (spectrum not shown) indicates the formation of surface carbonates, carboxylates, or related species on MgO (32). However, the bands observed at 1448 and 1160 cm^{-1} might indicate ν_{CC} and δ_{CH} vibrations, respectively, in the C_5H_5 and PhCN ligands of $\{Pt[W(CO)_3(C_5H_5)]_2(PhCN)_2\}$ (33, 34).

Treatment of the MgO-supported $\{Pt[W(CO)_3(C_5H_5)]_2 \cdot (PhCN)_2\}$ with H_2 at 400°C led to the disappearance of the carbonyl and organic ligands of the precursor.

Chemisorption and metal dispersion. The chemisorption data characterizing $(PtW_2)/MgO$ and $(Pt + W)/MgO$ after reduction at 400°C are compared in Tables 2–4 with those characterizing Pt/MgO (21). The amount of chemisorption of hydrogen or of CO on the sample prepared from $\{Pt[W(CO)_3(C_5H_5)]_2(PhCN)_2\}$ was less than that observed for Pt/MgO (Table 2). The electron micrographs characterizing the $(PtW_2)/MgO$ treated in H_2 at 400°C are similar to those of MgO itself. This result indicates the absence of observable Pt clusters or particles (roughly 10 Å in diameter or larger). Thus we conclude that the Pt dispersion was nearly 100%; from the hydrogen and CO chemisorption data we infer that the coverage of the Pt did not exceed 20% (Table 2).

Treatment of $(PtW_2)/MgO$ with O_2 at 200°C, followed by reduction with H_2 at 400°C, did not change the Pt dispersion. Nor was the uptake of hydrogen or CO sensitive to the O_2 treatment at this temperature (Table 3). These results again indicate a resistance of the metal in this sample to sintering in H_2 and O_2 atmospheres at temperatures up to 200°C. Only treatment with O_2 at 400°C, followed by reduction with H_2 at 400°C, led to increasing Pt surface coverage by H_2 or CO as a result of decreasing Pt dispersion (Table 3).

A different pattern was observed for $(Pt + W)/MgO$. The images recorded after treatment in H_2 at 400°C show 10–50 Å Pt particles with a surface-averaged size (d_{Pt}) of 24 Å. Treatment of this sample with O_2 at 200°C, followed by

TABLE 2

Chemisorption Properties of the MgO-Supported Pt Catalysts Reduced with H_2 at 400°C

Precursor(s)	Adsorption at 25°C, atomic ratio[a]		Pt_s/Pt_t[b]	Q_H[c]	Q_{CO}[c]	Reference
	H/Pt	CO/Pt				
$[PtCl_2(PhCN)_2]$	0.50	0.54	0.54	0.93	1.00	(21)
$[PtCl_2(PhCN)_2]+[W(CO)_6]$	0.19	0.28	0.47	0.40	0.60	This work
$[Pt[W(CO)_3(C_5H_5)]_2(PhCN)_2]$	0.13	0.20	1.00	0.13	0.20	This work

[a] Determined with respect to total number of Pt atoms in the sample.
[b] Dispersion expressed as the ratio of the number of surface atoms to total number of metal atoms in the sample.
[c] Fraction of the surface atoms covered by hydrogen or CO.

treatment in H_2 at 400°C, led to coalescence of the particles, with d_{Pt} increasing to 32 Å. The dispersions are summarized in Tables 2 and 3. Using the Pt dispersions determined by TEM, we estimate from the chemisorption data a hydrogen or CO coverage of 40–60% for the Pt surface after reduction at 400°C and a coverage of about 100% after treatment by O_2 at 200°C followed by reduction at 400°C.

The O_2 chemisorption and hydrogen titration data provide information about the oxidation state of W (Table 4). The O/W atomic ratio for the sample prepared from $[W(CO)_6]$ and treated in H_2 at 400°C was found to be 0.47. Oxygen chemisorbed on W/MgO was not removed during hydrogen titration, even at 200°C. Taking into account that the maximum oxidation state of W is +6, we deduce that the average oxidation state after reduction at 400°C was +5.1.

The oxygen uptakes by the samples prepared from $\{Pt[W(CO)_3(C_5H_5)]_2(PhCN)_2\}$ and from $[PtCl_2(PhCN)_2]+[W(CO)_6]$ and treated in H_2 at 400°C, represented as the O/Pt atomic ratio, were 1.14 and 1.08, respectively. These values exceed the stoichiometric oxygen adsorption reported for Pt/MgO (21). Since the W/MgO itself irreversibly adsorbs oxygen after reduction at this temperature, we suggest that the excess oxygen oxidized W cations. The amount of oxygen adsorbed by W cations was calculated as the difference between the total oxygen uptake by the sample and the amount adsorbed by Pt, determined from hydrogen titration data. The average oxidation states of W in the (PtW_2)/MgO and (Pt + W)/MgO samples, after reduction at 400°C, were found to be 5.1 and 5.3, respectively (Table 4).

Infrared spectra of CO adsorbed on MgO-supported samples. When (PtW_2)/MgO prereduced by H_2 at 400°C was exposed to CO at room temperature, ν_{CO} bands assigned to linear and bridging CO (35–43) appeared at 2069 and 1827 cm^{-1}, respectively (Fig. 2). Raising the temperature in flowing He to 140°C shifted the linear CO band to 2053 cm^{-1} without a substantial intensity change; the bridging CO band decreased in intensity and shifted to 1777 cm^{-1}. When

TABLE 3

Influence of Oxygen Treatment on Chemisorption Properties of the Pt Samples Reduced at 400°C

Precursor(s)	Temperature of treatment in O_2 (°C)[a]	Chemisorption at 25°C, atomic ratio		Pt_s/Pt_t[b]	Q_H[c]	Q_{CO}[c]
		H/Pt	CO/Pt			
$[PtCl_2(PhCN)_2]+[W(CO)_6]$	no treatment	0.19	0.28	0.47	0.40	0.60
	200	0.35	0.33	0.35	1.00	0.94
	300	0.38	0.35	—	—	—
	400	0.37	0.39	—	—	—
$[Pt[W(CO)_3(C_5H_5)]_2(PhCN)_2]$	no treatment	0.13	0.20	1.00	0.13	0.20
	200	0.16	0.21	1.00	0.16	0.21
	300	0.19	0.24	—	—	—
	400	0.25	0.26	0.35[d]	0.71	0.74

[a] Samples were treated in 10% O_2 in He.
[b] Dispersion expressed as the ratio of the number of surface atoms to total number of metal atoms in the sample was calculated on the basis of the TEM.
[c] Fraction of the surface atoms covered by hydrogen or CO.
[d] Estimated from EXAFS data.

TABLE 4

Oxygen Chemisorption and Hydrogen Titration Data for MgO-supported Pt Catalysts

Precursor(s)	Composition (wt%)	Reduction temperature (°C)	H/Pt[a]	O/Pt[b]	Hydrogen titration[c]	O/Pt[d]	O/W[e]	N_W[f]	Reference
$[W(CO)_6]$	2.0% W	400	—	—	0.0	—	0.47	5.1	This work
$[PtCl_2(PhCN)_2]$	1.0% Pt	400	0.50	0.97	1.62	0.54	—	—	(21)
$[PtCl_2(PhCN)_2]+[W(CO)_6]$	1.0% Pt 2.0% W	400	0.35	1.08	1.04	0.35	0.34	5.3	This work
$[Pt[W(CO)_3(C_5H_5)]_2(PhCN)_2]$	1.0% Pt 1.89% W	400	0.16	1.14	0.62	0.23	0.45	5.1	This work

[a] H/Pt values were determined after oxygen chemisorption followed by hydrogen titration and reduction of the catalyst at stated temperature.

[b] Total oxygen uptake, O/Pt atomic ratio, determined at 200°C.

[c] Amount of hydrogen required for titration of chemisorbed oxygen was determined at 200°C for the first sample and at 25°C for all of the other samples, H/Pt atomic ratio.

[d] Calculated from hydrogen titration data at room temperature taking into account the hydrogen chemisorption data.

[e] Amount of oxygen used for W oxidation in bimetallic samples, determined as the difference between the amount of oxygen chemisorbed by the sample and the amount of oxygen chemisorbed by Pt (determined from hydrogen titration data).

[f] Average W oxidation state determined from the equation $N_W = 6-2(O/W)$.

the temperature was ramped to 200°C, the intensity of each CO band decreased without further changes in position. No ν_{CO} bands remained at 200°C.

Similarly, when CO was adsorbed on (Pt + W)/MgO prereduced by H_2 at 400°C, the ν_{CO} bands assigned to linear and bridging CO were observed at 2072 and 1826 cm^{-1}, respectively (Fig. 3). When the temperature was ramped from 25 to 100°C with the sample in flowing He, the bridging CO band shifted to 1783 cm^{-1} and decreased in intensity. It disappeared at 110°C. Simultaneously, the linear CO band shifted to 2061 cm^{-1} and decreased in intensity without a further change in frequency. No ν_{CO} bands remained at 130°C (Fig. 3).

Toluene hydrogenation catalysis. The results for this reaction in the presence of MgO-supported Pt-containing catalysts prepared from various organometallic precursors (including organomolybdenum precursors) and prereduced by H_2 at 400°C are summarized in Table 5. Data are included in Table 5 for samples (21) prepared from $[PtCl_2(PhCN)_2]$, the mixture of $[PtCl_2(PhCN)_2]+[Mo(CO)_6]$, and $\{Pt[Mo(CO)_3(C_5H_5)]_2(PhCN)_2\}$. All the supported catalysts are characterized by approximately the same activation energies for toluene hydrogenation,

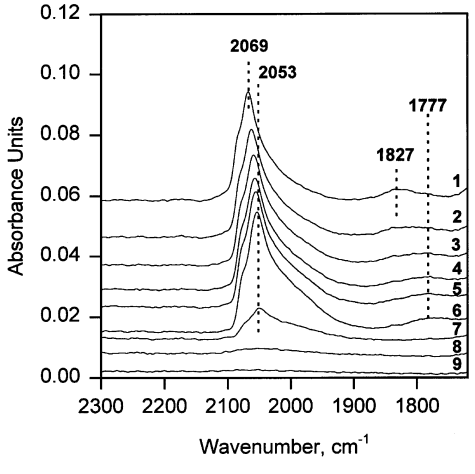

FIG. 2. Infrared spectra of CO adsorbed on sample prepared from $\{Pt[W(CO)_3(C_5H_5)]_2(PhCN)_2\}$ on MgO and reduced with H_2 at 400°C, following treatment in He under the following conditions: (1) 25°C; (2) 60°C; (3) 80°C; (4) 100°C; (5) 120°C; (6) 140°C; (7) 160°C; (8) 180°C; (9) 200°C.

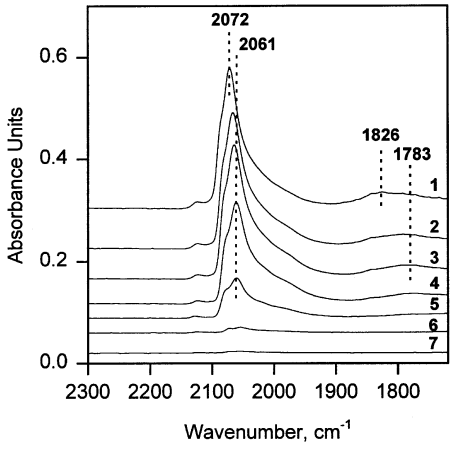

FIG. 3. Infrared spectra of CO adsorbed on sample (Pt + W)/MgO prepared from $[PtCl_2(PhCN)_2]+[W(CO)_6]$ on MgO and reduced with H_2 at 400°C, following treatment in He under the following conditions: (1) 25°C; (2) 60°C; (3) 80°C; (4) 100°C; (5) 110°C; (6) 120°C; (7) 130°C.

TABLE 5

Toluene Hydrogenation Catalyzed by MgO-Supported Catalysts Containing Pt

Precursor(s)	Temperature of treatment with H_2 (°C)	Activity, TOF × 10^3 (s^{-1})[a]	Apparent activation energy (kcal/mol)
$[PtCl_2(PhCN)_2]$	400	51.1	13.3
$[PtCl_2(PhCN)_2]+[Mo(CO)_6]$	400	54.2	11.2
$[PtCl_2(PhCN)_2]+[W(CO)_6]$	400	36.6	13.0
$[Pt[Mo(CO)_3(C_5H_5)]_2(PhCN)_2]$	400	4.0	11.5
$[Pt[W(CO)_3(C_5H_5)]_2(PhCN)_2]$	400	3.1	12.6

[a] Reaction at 60°C, $P_{toluene} = 50$ Torr and $P_{hydrogen} = 710$ Torr.

11–13 kcal/mol, agreeing with that reported for toluene hydrogenation catalyzed by supported Pt (44, 45). Turnover numbers were calculated on the basis of dispersion, determined by TEM.

The turnover frequency observed for (Pt + W)/MgO was found to be about the same as that observed for the sample prepared from $[PtCl_2(PhCN)_2]$ without Mo or W; in contrast, the turnover frequency observed for the sample prepared from $\{Pt[Mo(CO)_3(C_5H_5)]_2(PhCN)_2\}$ was an order of magnitude less. The same trend was observed for the W-containing samples. The turnover frequency observed the sample prepared from $[PtCl_2(PhCN)_2]+[W(CO)_6]$ was about 28% less than that for Pt/MgO, whereas that observed for the sample prepared from $\{Pt[W(CO)_3(C_5H_5)]_2(PhCN)_2\}$ was more than an order of magnitude less than that for Pt/MgO.

EXAFS data. The parameters determined by fitting are summarized in Tables 6–13, and the comparisons of the data and the fits, both in *k* space and in *r* space, are shown in Figs. 4–6. The residual spectra determined by subtracting the Pt–Pt + $Pt–O_{support}$ contributions from the raw EXAFS data for the Pt L_{II} edge and by subtracting the W–W + $W–O_{support}$ contributions from the raw EXAFS data for the W L_{III} edge (which gives evidence of the Pt–W and W–Pt interactions, respectively) are shown in Figs. 5D and 6D, respectively. The XDAP software was used to obtain rough estimates of the error bounds in the EXAFS parameters, as shown in Tables 6–13. These error bounds represent precisions determined from statistical analysis of the data, not accuracies.

TABLE 6

EXAFS Results at the Pt L_{II} Edge Characterizing the MgO- Supported Sample (Pt + W)/MgO Prepared from $[PtCl_2(PhCN)_2]+[W(CO)_6]$ after Treatment in H_2 at 400°C for 2 h[a]

Shell	N	R (Å)	$10^3\times\Delta\sigma^2$ ($Å^2$)	ΔE_0 (eV)	EXAFS reference
Pt–Pt	7.0 ± 0.4	2.72 ± 0.01	1.1 ± 0.4	5.7 ± 0.5	Pt–Pt
$Pt–O_{support}$					
$Pt–O_s$	0.9 ± 0.1	2.18 ± 0.01	-2.6 ± 0.7	-12.1 ± 0.7	Pt–O
$Pt–O_l$	1.1 ± 0.2	2.67 ± 0.02	10.0 ± 3.9	-7.9 ± 1.8	Pt–O

[a] Notation: N, coordination number; R, distance between absorber and backscatterer atom; $\Delta\sigma^2$, Debye–Waller factor; ΔE_0, inner potential correction.

TABLE 7

EXAFS Results at the Pt L_{II} Edge Characterizing the MgO- Supported Sample (Pt + W)/MgO Prepared from $[PtCl_2(PhCN)_2]+[W(CO)_6]$ Following Treatment in O_2 at 200°C for 1 h and Then in H_2 at 400°C for 2 h[a]

Shell	N	R (Å)	$10^3\times\Delta\sigma^2$ ($Å^2$)	ΔE_0 (eV)	EXAFS reference
Pt–Pt	8.0 ± 0.3	2.72 ± 0.01	0.3 ± 0.2	5.9 ± 0.3	Pt–Pt
$Pt–O_{support}$					
$Pt–O_s$	0.7 ± 0.1	2.20 ± 0.01	-7.81 ± 0.3	-10.2 ± 0.7	Pt–O
$Pt–O_l$	1.1 ± 0.2	2.67 ± 0.02	10.0 ± 3.0	-7.2 ± 1.9	Pt–O

[a] Notation as in Table 6.

DISCUSSION

Interaction of $\{Pt[W(CO)_3(C_5H_5)]_2(PhCN)_2\}$ with MgO. Although the preparation of MgO-supported catalysts from organometallic precursors has been reported by a number of authors (46–50), the chemistry of interactions of organometallic compounds with the basic MgO is still not as well developed as that with neutral or acidic supports (11). However, the interactions of metal carbonyls with MgO are relatively well understood. Often metal carbonyl clusters react with OH groups of MgO to form supported metal carbonyl cluster anions (46, 47); anion formation manifests itself ν_{CO} band shifts. Alternatively, metal carbonyls interact with coordinatively unsaturated Mg^{2+} ions through CO ligands bridging metal atoms of the cluster and Mg^{2+} of the support, leading to the appearance of broad ν_{CO} bands in the region 1800–1600 cm^{-1} (48).

Little is known about the interactions of organometallic compounds incorporating hydrocarbon ligands with MgO. Some such organometallics are adsorbed intact, but

TABLE 8

EXAFS Results at the Pt L_{II} Edge Characterizing the MgO-Supported Sample (PtW_2)/MgO Prepared from $\{Pt[W(CO)_3\cdot(C_5H_5)]_2(PhCN)_2\}$ after Treatment in H_2 at 400°C for 2 h[a]

Shell	N	R (Å)	$10^3\times\Delta\sigma^2$ ($Å^2$)	ΔE_0 (eV)	EXAFS reference
Pt–Pt	3.0 ± 0.2	2.72 ± 0.01	0.0 ± 0.5	7.4 ± 0.3	Pt–Pt
Pt–W	2.1 ± 0.2	2.71 ± 0.01	2.5 ± 0.5	-19.5 ± 0.9	Pt–W
$Pt–O_{support}$					
$Pt–O_s$	1.9 ± 0.1	2.17 ± 0.01	9.1 ± 0.6	-7.5 ± 0.3	Pt–O
$Pt–O_l$	3.8 ± 0.1	2.71 ± 0.01	9.8 ± 1.0	-9.6 ± 0.7	Pt–O

[a] Notation as in Table 6.

TABLE 9

EXAFS Results at the W L_{III} Edge Characterizing the MgO-Supported Sample $(PtW_2)/MgO$ Prepared from $\{Pt[W(CO)_3(C_5H_5)]_2(PhCN)_2\}$ after Treatment in H_2 at 400°C for 2 h[a]

Shell	N	R (Å)	$10^3 \times \Delta\sigma^2$ (Å^2)	ΔE_0 (eV)	EXAFS reference
W–W	2.3 ± 0.3	3.02 ± 0.02	9.6 ± 1.1	-10.0 ± 1.1	W–W
W–Pt	1.1 ± 0.2	2.71 ± 0.01	2.7 ± 0.5	-1.9 ± 0.9	W–Pt
W–$O_{support}$					
W–O_s	0.8 ± 0.1	1.93 ± 0.01	0.5 ± 0.4	13.9 ± 0.7	W–O
W–O_l	2.3 ± 0.3	2.70 ± 0.02	10.0 ± 1.1	13.4 ± 1.5	W–O

[a] Notation as in Table 6.

TABLE 11

EXAFS Results at the W L_{III} Edge Characterizing the MgO-Supported Sample $(PtW_2)/MgO$ Prepared from $\{Pt[W(CO)_3(C_5H_5)]_2(PhCN)_2\}$ Following Treatment in O_2 at 200°C for 1 h and Then in H_2 at 400°C for 2 h[a]

Shell	N	R (Å)	$10^3 \times \Delta\sigma^2$ (Å^2)	ΔE_0 (eV)	EXAFS reference
W–Pt	0.8 ± 0.1	2.71 ± 0.01	3.4 ± 0.2	-4.0 ± 0.7	W–Pt
W–$O_{support}$					
W–O_s	1.6 ± 0.1	1.90 ± 0.01	3.3 ± 0.1	19.2 ± 0.2	W–O
W–O_l	0.7 ± 0.1	2.64 ± 0.02	1.8 ± 0.3	-5.6 ± 0.4	W–O
W–O_{l2}	3.1 ± 0.1	2.83 ± 0.02	9.7 ± 0.3	0.7 ± 0.3	W–O

[a] Notation as in Table 6.

structural changes often result from adsorption (49, 50). For example, $[Rh(C_3H_5)_3]$ decomposed on MgO, giving Rh particles (49), whereas $[Pt(C_3H_5)_2]$ was supported intact on MgO (although treatment in H_2 readily converted this precursor into Pt particles) (50).

The results presented here show that adsorption of $\{Pt[W(CO)_3(C_5H_5)]_2(PhCN)_2\}$ on MgO caused the color of the solid to change from white to brown, with the appearance of new bands in the infrared spectrum at 3115, 3067, and 2958 cm^{-1} (attributed to ν_{CH}) and at 1448 and 1160 cm^{-1} (attributed, respectively, to ν_{CC} and δ_{CH} of C_5H_5 and PhCN ligands) (33, 34). Bands observed at 2052, 1980, 1943, 1857, and 1831 cm^{-1} are attributed (23, 24) to carbonyl ligands (Figs. 1A and 1B). The observation of nearly the same band positions of the carbonyl ligands, before and after adsorption of $\{Pt[W(CO)_3(C_5H_5)]_2(PhCN)_2\}$ with MgO, indicates that decomposition of this precursor did not take place and that anionic clusters were not formed. The appearance of a broad absorption band centered at about 3640 cm^{-1} (Fig. 1A) indicates the formation of hydrogen-bonded species on the MgO surface. The shift of the OH absorption bands was about 100 cm^{-1}, which is within the range expected for alkenes interacting with surface OH groups (32). We infer that (unidentified) hydrogen-bonded species formed by the interaction of organic ligands of $\{Pt[W(CO)_3(C_5H_5)]_2(PhCN)_2\}$ with surface OH groups. Similarly, hydrogen-bonded surface species were formed from $[Zr(\pi\text{-}C_3H_5)_4]$ on SiO_2 (51). The appearance of bands at about 1700–1200 cm^{-1}, attributed to surface metal carbonates or metal carboxyl-like species (30), is explained by the interactions of the carbonyl ligands of $\{Pt[W(CO)_3(C_5H_5)]_2(PhCN)_2\}$ with O^{2-} ions of $\{Mg^{2+}O^{2-}\}$ acid-base pairs, as had been suggested for $[Fe(CO)_5]$ on MgO (52).

In summary, the anchoring of $\{Pt[W(CO)_3(C_5H_5)]_2(PhCN)_2\}$ to the MgO surface is attributed to weak interactions of organic ligands of the cluster with surface OH groups and interaction of terminal carbonyl ligands with surface O^{2-} ions, with formation of hydrogen-bonded OH groups and metal carbonate or metal carboxyl-like species. Thus we infer that the metal frame of the precursor was preserved on the support.

Dispersion and chemisorptive properties of MgO-supported samples containing Pt. The TEM results show that Pt particles about 24 Å in average diameter were formed in (Pt + W)/MgO after treatment in H_2 at 400°C. The Pt dispersion calculated from the TEM data was about the same as that reported for Pt/MgO after treatment under similar conditions (Table 2) (21). The Pt–Pt first-

TABLE 10

EXAFS Results at the Pt L_{II} Edge Characterizing the MgO-Supported Sample $(PtW_2)/MgO$ Prepared from $\{Pt[W(CO)_3(C_5H_5)]_2(PhCN)_2\}$ Following Treatment in O_2 at 200°C for 1 h and Then in H_2 at 400°C for 2 h[a]

Shell	N	R (Å)	$10^3 \times \Delta\sigma^2$ (Å^2)	ΔE_0 (eV)	EXAFS reference
Pt–Pt	5.4 ± 0.2	2.72 ± 0.01	1.9 ± 0.3	10.8 ± 0.6	Pt–Pt
Pt–W	2.0 ± 0.2	2.71 ± 0.01	3.0 ± 0.6	-19.7 ± 1.2	Pt–W
Pt–$O_{support}$					
Pt–O_s	2.6 ± 0.1	2.10 ± 0.01	0.6 ± 0.3	0.4 ± 0.2	Pt–O
Pt–O_l	3.3 ± 0.1	2.67 ± 0.01	6.6 ± 0.8	-6.3 ± 0.6	Pt–O

[a] Notation as in Table 6.

TABLE 12

EXAFS Results at the Pt L_{II} Edge Characterizing the MgO-Supported Sample $(PtW_2)/MgO$ Prepared from $\{Pt[W(CO)_3(C_5H_5)]_2(PhCN)_2\}$ Following Treatment in O_2 at 400°C for 1 h and Then in H_2 at 400°C for 2 h[a]

Shell	N	R (Å)	$10^3 \times \Delta\sigma^2$ (Å^2)	ΔE_0 (eV)	EXAFS reference
Pt–Pt	7.7 ± 0.1	2.74 ± 0.01	-0.4 ± 0.2	7.3 ± 0.1	Pt–Pt
Pt–W	2.2 ± 0.1	2.71 ± 0.01	5.0 ± 0.3	-19.5 ± 0.4	Pt–W
Pt–$O_{support}$					
Pt–O_s	1.8 ± 0.1	2.20 ± 0.01	7.9 ± 0.5	-7.6 ± 0.2	Pt–O
Pt–O_l	3.5 ± 0.2	2.66 ± 0.01	10.0 ± 1.1	-6.8 ± 0.3	Pt–O

[a] Notation as in Table 6.

TABLE 13

EXAFS Results at the W L_{III} Edge Characterizing the MgO-Supported Sample (PtW_2)/MgO Prepared from {$Pt[W(CO)_3 \cdot (C_5H_5)]_2(PhCN)_2$} Following Treatment in O_2 at 400°C for 1 h and Then in H_2 at 400°C for 2 h[a]

Shell	N	R (Å)	$10^3 \times \Delta\sigma^2$ (Å^2)	ΔE_0 (eV)	EXAFS reference
W–Pt	0.9 ± 0.2	2.71 ± 0.01	4.9 ± 0.2	-2.2 ± 0.7	W–Pt
$W–O_{support}$					
$W–O_s$	1.6 ± 0.1	1.90 ± 0.01	3.3 ± 0.4	19.2 ± 0.2	W–O
$W–O_l$	0.8 ± 0.1	2.66 ± 0.02	0.11 ± 0.3	-6.5 ± 0.4	W–O
$W–O_{l2}$	3.1 ± 0.1	2.83 ± 0.02	9.3 ± 0.3	0.7 ± 0.3	W–O

[a] Notation as in Table 6.

shell EXAFS coordination number characterizing the former sample after reduction at 400°C was about 7.0 (Table 6), consistent with TEM results and indicating that aggregation of the Pt resulted from the treatment in H_2. A comparison of the Pt dispersion in this sample with the amounts of adsorbed hydrogen (or CO) indicates that the coverage of surface Pt atoms by these adsorbates was roughly 50% (Table 2).

In contrast, the TEM data give evidence that much smaller Pt clusters were formed in (PtW_2)/MgO (Table 2). The EXAFS data confirm this conclusion. The Pt–Pt first-shell coordination number was about 3.0 after reduction at 400°C (Table 8), which indicates Pt clusters with an average of only about 4 atoms each. There was markedly less adsorption of hydrogen or of CO on the highly dispersed (PtW_2)/MgO than on Pt/MgO (Table 2). The surface coverage by hydrogen or by CO was only about 20% in the former sample. The data are consistent with a report (11) of the effect of W on the chemisorptive properties of Pt, attributed to W–Pt interactions.

There was relatively little chemisorption on either (PtW_2)/MgO or (Pt + W)/MgO. The effect of W in reducing the chemisorption on Pt is greater for the former sample than the latter (Table 2). Furthermore, the effect of W in helping to maintain a high dispersion was greater for the former sample than for the latter, as shown by the TEM and EXAFS data. We infer that the interactions between Pt atoms and W cations, which were originally bonded to each other in the bimetallic precursor, helps to stabilize the Pt dispersion in (PtW_2)/MgO after treatment in H_2.

Treatment of (Pt + W)/MgO with O_2 at 200°C and then H_2 at 400°C lowered the Pt dispersion and increased the Pt surface coverage by hydrogen or by CO to 100% (Table 3), consistent with the formation of larger Pt particles. The EXAFS data are consistent with this conclusion, showing that the Pt–Pt first-shell coordination number was about 8.0 after this treatment (Table 7).

In contrast, the TEM data show that similar treatment of (PtW_2)/MgO with O_2 did not change the Pt dispersion, and changes in the coverage of Pt by hydrogen or by CO were insignificant in comparison with those observed for (Pt + W)/MgO (Table 3). However, the EXAFS data show that the Pt–Pt first-shell coordination number was larger (about 5.4) after the treatment with O_2 at 200°C than after treatment with only H_2 (Table 10). The average Pt cluster size in (PtW_2)/MgO can be estimated roughly from the EXAFS data (53). If it is assumed that the clusters are just Pt and spherical with a fcc structure (which is an oversimplification), the Pt–Pt first-shell coordination number of 5.4 implies that the Pt clusters after treatment in O_2 at 200°C and H_2 at 400°C contained about 20 atoms each, on average; these are too small to observe by TEM, in agreement with the observations. After the treatment of this sample with O_2 at 400°C the Pt–Pt first-shell coordination number was about 7.7 (Table 12), which is about the same as that determined for (Pt + W)/MgO after the treatment with only H_2 at 400°C. These results suggest that Pt tends to sinter under oxidizing conditions but much less than in (Pt + W)/MgO.

Thus the results demonstrate that the Pt–W interactions in (Pt + W)/MgO were weaker than those in (PtW_2)/MgO; these interactions can evidently be weakened by O_2 treatment, as shown by the increased coverage of Pt by hydrogen and by CO observed following this treatment. The chemisorption data also show that the Pt–W interactions in (PtW_2)/MgO were strong enough to largely maintain the structures of the supported bimetallic clusters even in an oxidizing atmosphere.

State of W in reduced samples. Oxygen chemisorption in combination with titration of preadsorbed oxygen with H_2 (hydrogen titration) is often used (with an assumed stoichiometry of hydrogen titration) to estimate the dispersion of supported Pt and Pd (54). However, when a noble metal is combined with another metal on a support, the chemisorptive properties of the noble metal may change, so that hydrogen chemisorption no longer provides a good measure of the dispersion (55). Hence, chemisorption is not generally reliable for determination of metal cluster or particle sizes in bimetallic samples. Nevertheless, when combinations of noble and oxophilic metals are examined, oxygen chemisorption followed by hydrogen titration allows at least a rough estimate of the oxidation state of the oxophilic metal. The determination is based on the tendency of supported oxophilic metals such as Mo, W, Ti, Zr, after treatment in H_2, to form coordinatively unsaturated cations in lower oxidation states on the support surface, which irreversibly adsorb oxygen during oxidation. Both the degree of cation reduction and the structure of the surface species depend on the treatment temperature (11). The chemisorption data (Table 4) for the sample prepared from $[W(CO)_6]$ on MgO and reduced with H_2 at 400°C illustrate this point. Assuming that oxidation leads to formation of W^{6+} cations, we infer from the O_2 uptake that the average W oxidation state reduction at 400°C was about +5. Similar data were

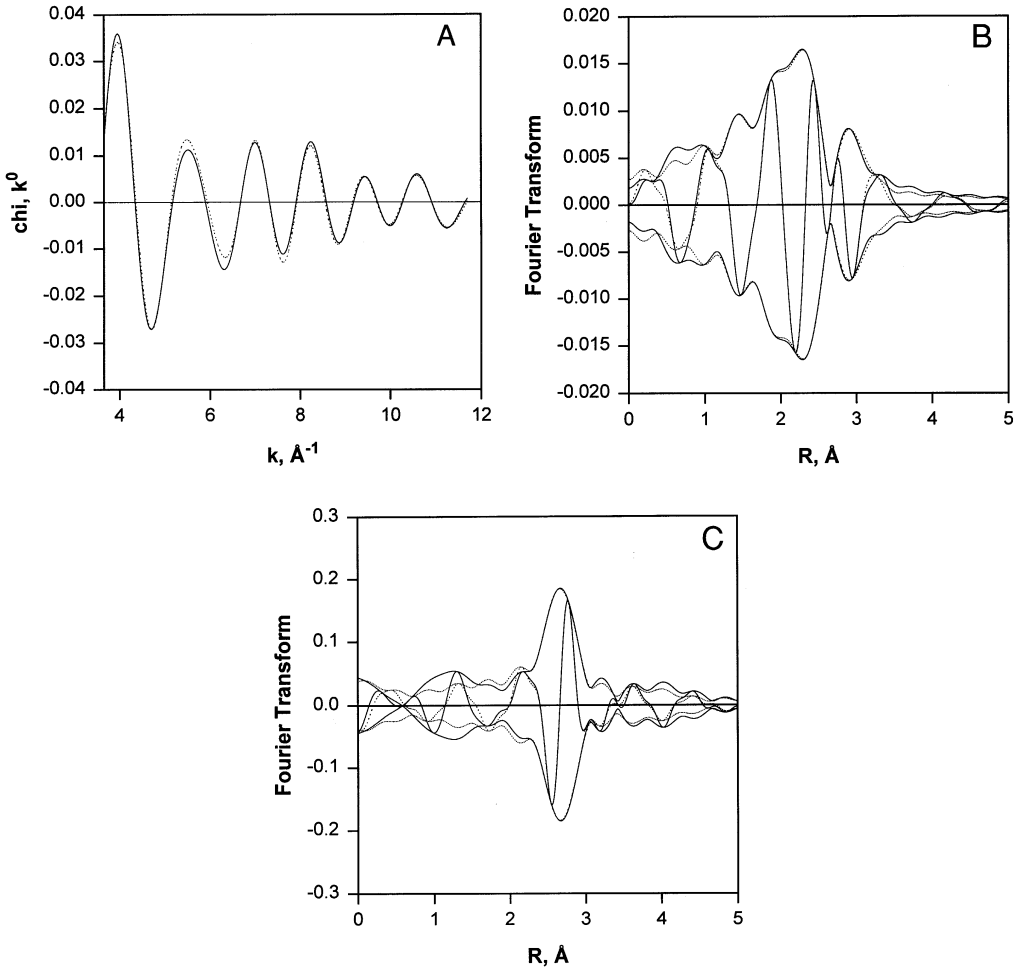

FIG. 4. Results of EXAFS analysis near the Pt L_{II} edge obtained with the best calculated coordination parameters characterizing the MgO-supported sample (Pt + W)/MgO prepared from $[PtCl_2(PhCN)_2] + [W(CO)_6]$ precursors following treatment in H_2 at 400°C: (A) experimental EXAFS (solid line) and sum of the calculated Pt–Pt + Pt–O_s + Pt–O_l contributions (dotted line); (B) imaginary part and magnitude of uncorrected Fourier transform (k^0 weighted) of experimental EXAFS (solid line) and sum of the calculated Pt–Pt + Pt–O_s + Pt–O_l contributions (dotted line); (C) imaginary part and magnitude of phase- and amplitude-corrected Fourier transform (k^0 weighted) of raw data minus the calculated Pt–O_s + Pt–O_1 contributions (solid line) and calculated Pt–Pt contribution (dotted line).

reported (21) for the sample prepared from $[Mo(CO)_6]$ and treated under the same conditions. The results of hydrogen titration show that the chemisorbed oxygen atoms are strongly bonded to the cations and do not react with H_2 at temperatures up to 200°C. Thus, it is possible to distinguish oxygen adsorbed on an oxophilic metal from that adsorbed on a noble metal, which can be easily removed by hydrogen titration.

The total oxygen uptakes (represented as the O/Pt atomic ratio) characteristic of (Pt + W)/MgO and (PtW_2)/MgO were somewhat larger than the value for Pt/MgO. Because the former samples incorporate W in addition to Pt, we infer that some of the chemisorbed oxygen was bonded to Pt, with the remainder oxidizing W cations (Table 4). The average oxidation state of W, determined from the O/W values, was about +5 for each sample. It has been shown (21) that close proximity of Mo cations to Pt in the sample prepared from $\{Pt[Mo(CO)_3(C_5H_5)]_2(PhCN)_2\}$ led to deeper reduction of Mo than in a sample prepared from $[PtCl_2(PhCN)_2] + [Mo(CO)_6]$, in which Pt and Mo were largely segregated. The data reported here for W-containing samples, together with those reported elsewhere (21), show that the higher the atomic number of the oxophilic metal, the higher the temperature required to reduce the metal to a low oxidation state. Substantial reduction of W in W/SiO_2 was observed only at temperatures as high as about 600°C (11).

CO chemisorption on Pt-containing samples: Evidence from infrared spectroscopy. Evidence of CO chemisorption and the stability of the different forms of adsorbed CO as a function of temperature are provided by the data

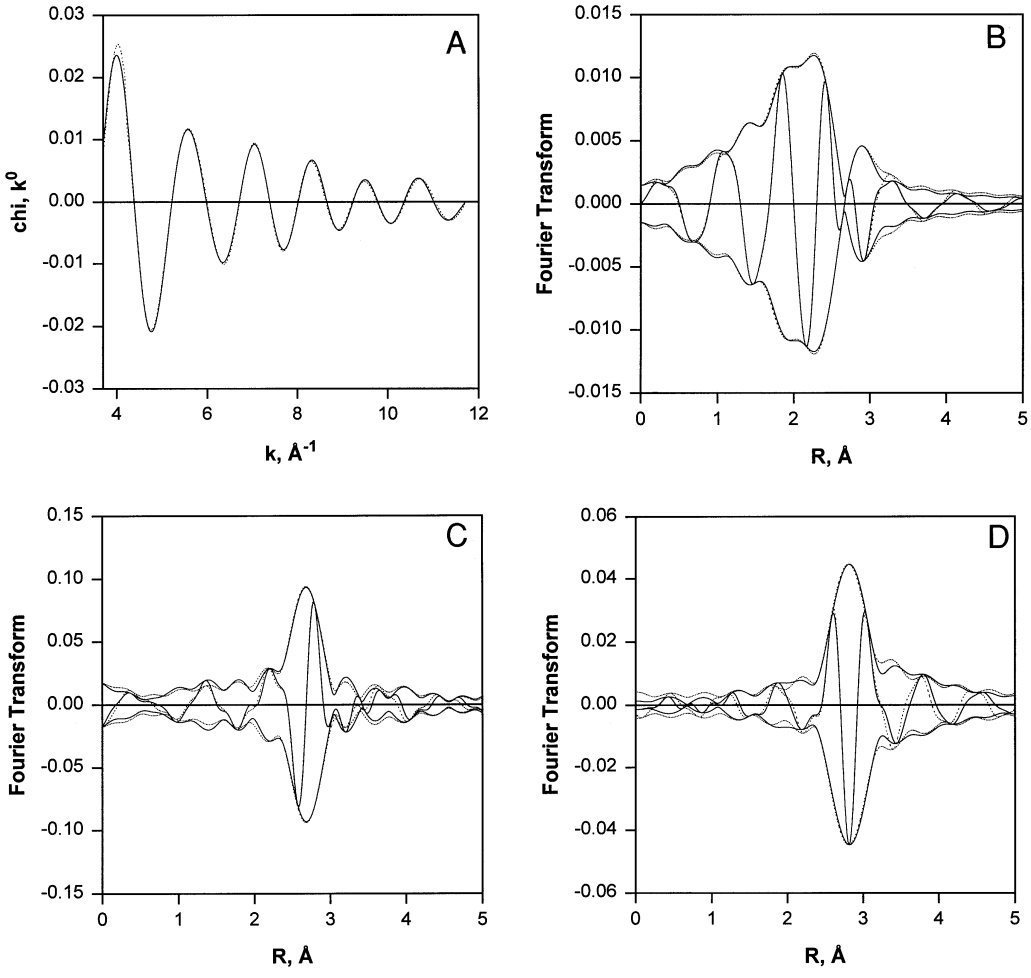

FIG. 5. Results of EXAFS analysis near the Pt L_{II} edge obtained with the best calculated coordination parameters characterizing the MgO-supported sample $(PtW_2)/MgO$ prepared from $\{Pt[W(CO)_3(C_5H_5)]_2(PhCN)_2\}$ following treatment in H_2 at 400°C: (A) experimental EXAFS (solid line) and sum of the calculated Pt–Pt + Pt–O_s + Pt–O_l + Pt–W contributions (dotted line); (B) imaginary part and magnitude of uncorrected Fourier transform (k^0 weighted) of experimental EXAFS (solid line) and sum of the calculated Pt–Pt + Pt–O_s + Pt–O_l + Pt–W contributions (dotted line); (C) imaginary part and magnitude of phase- and amplitude-corrected Fourier transform (k^0 weighted) of raw data minus the calculated Pt–O_s + Pt–O_l + Pt–W contributions (solid line) and calculated Pt–Pt contribution (dotted line); (D) residual spectrum illustrating the Pt–W contributions: imaginary part and magnitude of phase- and amplitude-corrected Fourier transform (k^0 weighted) of raw data minus calculated Pt–Pt + Pt–O_s + Pt–O_l EXAFS (solid line) and calculated Pt–W contribution (dotted line).

of Figs. 2 and 3. After treatment of (Pt + W)/MgO or of $(PtW_2)/MgO$ (that had been reduced with H_2 at 400°C) with CO flowing at 25°C, both linear and bridging CO bands were observed. The frequencies correspond to CO adsorption on completely reduced Pt sites, in agreement with the literature (35–43). Consistent with earlier observations (36, 37, 40), the bridging CO bands at about 1827 cm^{-1} are weak, constituting a small fraction of the CO band intensities; these were clearly evident only at high surface coverages and rapidly disappeared with increasing temperature for both samples (Figs. 2 and 3). These data indicate that the bridging CO is less stable than the terminal CO, which is explained by differences in bonding energy between these two forms of CO and Pt atoms (41).

The shift of the intense bands attributed to terminally bonded CO to 2061 and 2053 cm^{-1}, respectively, in the spectra of (Pt + W)/MgO and $(PtW_2)/MgO$ as the temperature increased was not accompanied by substantial decreases in band intensities. Such shifts have already been observed (38, 39) and may be explained by decreasing dipole–dipole coupling between adsorbed CO molecules with decreasing coverage. A comparison of ν_{CO} values in the infrared spectra recorded at high temperature (and low CO coverage) for (Pt + W)/MgO and $(PtW_2)/MgO$ with those reported for Pt/MgO (21) indicates that the frequency differences for the terminal CO were about 10 and 18 cm^{-1}, respectively.

The adsorption of CO on transition metals involves electron donation from CO 5σ orbitals to vacant *d*-orbitals of

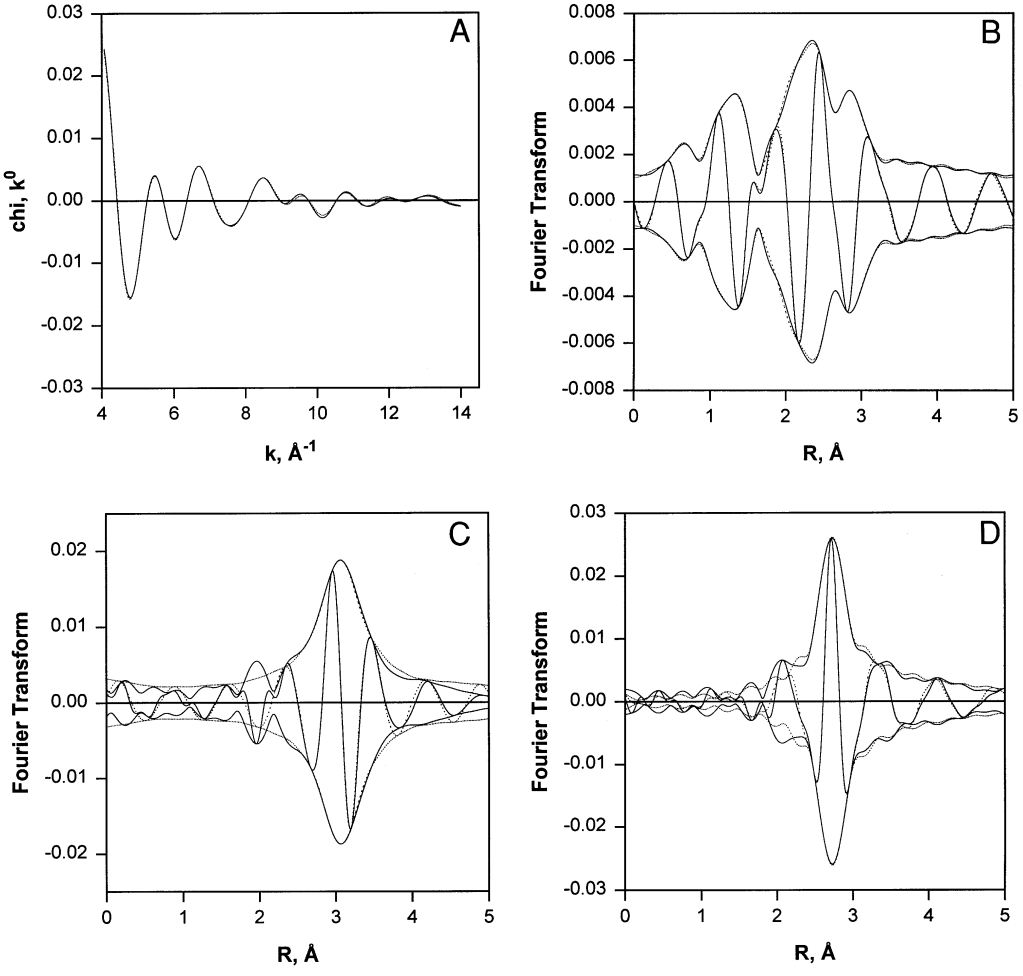

FIG. 6. Results of EXAFS analysis near the W L_{III} edge obtained with the best calculated coordination parameters characterizing the MgO-supported sample (PtW_2)/MgO prepared from $\{Pt[W(CO)_3(C_5H_5)]_2(PhCN)_2\}$ following treatment in H_2 at 400°C: (A) experimental EXAFS (solid line) and sum of the calculated W–W + W–O_s + W–O_l + W–Pt contributions (dotted line); (B) imaginary part and magnitude of uncorrected Fourier transform (k^0 weighted) of experimental EXAFS (solid line) and sum of the calculated W–W + W–O_s + W–O_l + W–Pt contributions (dotted line); (C) imaginary part and magnitude of phase- and amplitude-corrected Fourier transform (k^0 weighted) of raw data minus the calculated W–O_s + W–O_l + W–Pt contributions (solid line) and calculated W–W contribution (dotted line); (D) residual spectrum illustrating the W–Pt contributions: imaginary part and magnitude of phase- and amplitude-corrected Fourier transform (k^0 weighted) of raw data minus calculated W–W + W–O_s + W–O_l EXAFS (solid line) and calculated W–Pt contribution (dotted line).

the metal and back donation from filled *d*-orbitals of the metal to the CO $2\pi^*$ antibonding orbitals (56). Because of backbonding, changes in the electronic environment of the metal influence the *M*–CO bond strength and thereby the C–O stretching frequency. The infrared data indicate a greater back donation from Pt to CO in (PtW_2)/MgO than in (Pt + W)/MgO.

The infrared data show that higher temperatures were required to remove CO from (PtW_2)/MgO than from (Pt + W)/MgO. This pattern is one of increasing stability of adsorbed CO with increasing electron density on Pt and with increasing interactions between Pt and W cations. The pattern is explained by strengthening of Pt–CO bonds by increasing back donation of the metal electrons into CO $2\pi^*$ orbitals with simultaneous weakening of the C=O bond as a result of the presence of the second metal (57–59).

The infrared evidence of greater backbonding in (PtW_2)/MgO is in agreement with the results indicating greater Pt–W interactions in this sample than in (Pt + W)/MgO. Specifically, the Pt-edge EXAFS data for (PtW_2)/MgO (Table 8) indicate a substantial Pt–W interaction. The Pt–W first-shell coordination number was found to be about 2, with an average distance of 2.71 Å. The analysis of the W-edge EXAFS data for this sample gave a W–Pt first-shell coordination number of about 1.1 with an average distance of 2.71 Å (Table 9).

In contrast to the data characterizing (PtW_2)/MgO, which indicate strong Pt–W interactions, the Pt-edge EXAFS data

obtained for (Pt + W)/MgO (Table 6) give no evidence of Pt–W contributions. Taking account of both the EXAFS and infrared data, we infer that only a small fraction of the W cations were near neighbors of Pt in the sample.

Similar data for MgO-supported Pt–Mo samples show that proximity of Pt atoms and Mo cations leads to strong CO adsorption on Pt relative to that for a sample lacking Mo (21); the data are consistent with the Pt–W data reported here.

Structures of supported bimetallic catalysts. The EXAFS data provide evidence of the structure of the bimetallic clusters as well as a basis for comparing the bimetallic interactions in $(PtW_2)/MgO$ and (Pt + W)/MgO. The results characterizing the latter sample indicate an average Pt–Pt coordination number of 7.0 after reduction at 400°C (Table 6). In agreement with the TEM data, this result indicates relatively large Pt particles, in which each Pt atom had about 7 near Pt neighbors (the value for bulk Pt is 12). No Pt–W contribution was indicated by the EXAFS data for (Pt + W)/MgO; however, the chemisorption of hydrogen (or CO) on Pt was less than on Pt/MgO, which indicates a modification of the chemisorption properties of the Pt caused by the W cations. Treatment of this sample with O_2 led to a change in the Pt dispersion and chemisorptive properties; the Pt–Pt first-shell coordination number increased to about 8.0 with an average Pt–Pt distance of about 2.72 Å, which indicates Pt aggregation. The TEM data confirm this aggregation. The surface coverage of Pt by CO or by hydrogen was about 100% after O_2 treatment, and the results are about the same as those observed for chemisorption of these gases on Pt/MgO. Therefore, the data show that interactions of Pt atoms and W cations in this sample were weak and could easily be broken by O_2 treatment. Thus we infer that only a small fraction of the Pt atoms in this sample were near neighbors of W cations.

In contrast, the Pt-edge EXAFS results characterizing $(PtW_2)/MgO$ (Table 8) indicate an average Pt–Pt coordination number of only 3.0. This result is consistent with the TEM data and indicates the presence of Pt clusters of only about 4 atoms each, on average. Moreover, substantial Pt–W interactions are indicated by the EXAFS data, with each Pt atom, on average, being surrounded by about two near-neighbor W atoms at an average distance of 2.71 Å. Additional information about the Pt–W structures is provided by the W-edge EXAFS data (Table 9), which indicate substantial W–W interactions with an average W–W coordination number of 2.3 at a distance of 3.02 Å. The observed W–W distance is larger than that typically observed in metallic W (2.74 Å) and indicates interactions between W cations in W–O–W structures. The EXAFS data also indicate W–Pt interactions with an average W–Pt coordination number of 1.1 at a distance of 2.71 Å. The implication is that each W cation in this sample interacts, on average, with about two W cations and about one Pt atom. Thus the results indicate that the Pt–W interactions in $(PtW_2)/MgO$ were strong.

EXAFS spectroscopy determines average coordination parameters. The average Pt–W coordination number (N_{Pt-W}) might be described by the equation

$$N_{Pt-W} = \theta_{Pt-W}/n_{Pt_{tot}}, \quad [1]$$

where θ_{Pt-W} is the total number of Pt–W near neighbors, and $n_{Pt_{tot}}$ is the total number of Pt atoms in the sample. An equivalent statement can be made for the average W–Pt coordination number (N_{W-Pt}). Since the number of Pt–W near neighbors (θ_{Pt-W}) should be equal to the number of W–Pt near neighbors (θ_{W-Pt}), the relationship between N_{Pt-W} and N_{W-Pt} may be expressed as

$$N_{Pt-W}/N_{W-Pt} = n_{W_{tot}}/n_{Pt_{tot}}. \quad [2]$$

N_{Pt-W}/N_{W-Pt} was found to be equal to about 2, consistent with the stoichiometry of the precursor $\{Pt[W(CO)_3 \cdot (C_5H_5)]_2(PhCN)_2\}$.

Moreover, the bond distances (R) and Debye–Waller factors ($\Delta\sigma^2$) should be the same for the Pt–W and W–Pt EXAFS contributions. The result that these EXAFS parameters determined from the Pt edge data (Tables 8, 10, 12) and those determined from the W edge data (Tables 9, 11, 13) agree within the experimental errors shows the internal consistency of the data and justifies the validity of the fit.

After treatment of $(PtW_2)/MgO$ with O_2 at 200°C followed by reduction in H_2 at 400°C, the Pt–Pt first-shell coordination number was about 5.4 with an average distance of 2.71 Å. Further treatment of this sample with O_2 at 400°C followed by H_2 at 400°C led to an increase in the Pt–Pt first-shell coordination number to 7.7. In addition to Pt–Pt interactions, Pt–W contributions were observed after treatment of the sample with O_2. Within the approximate error bounds, the Pt–W first-shell coordination numbers and Pt–W distances were about the same as those determined for the sample after reduction at 400°C. The oxygen treatment led only to a systematic increase in the Debye–Waller factors for the Pt–W contributions, which indicates an increasing degree of disorder resulting from treatment at increasing temperatures under oxidizing conditions. The implication is that O_2 treatment led to some Pt sintering in this sample, but sintering occurred without substantial disruption of the Pt–W interactions; the degree of sintering was less than that observed for (Pt + W)/MgO.

The W-edge EXAFS data confirm this conclusion. The W–W contribution disappeared after O_2 treatment, concomitant with increasing W–O contributions. However, the W–Pt first-shell coordination numbers and distances were not sensitive to the treatment conditions, being virtually the same as those determined for this sample after reduction at 400°C. O_2 treatment also led to increasing Debye–Waller

factors for the W–Pt contributions, indicating an increasing degree of disorder, as was observed for the Pt edge data. These results, in agreement with the chemisorption data, show that the Pt–W interactions in (PtW_2)/MgO were strong and largely maintained under oxidizing conditions.

In addition to the metal–metal contributions mentioned above, the EXAFS data indicate metal–oxygen contributions, which we identify with metal-support interactions (Tables 8 and 9). We doubt that the EXAFS data are sufficient to justify a model of the structure of the metal–support interface, but they clearly show substantial interactions of both W cations and Pt atoms with oxygen atoms of the support.

Evidence of the role of W in stabilizing the dispersion of Pt in MgO-supported samples is in accord with TEM, chemisorption, and EXAFS evidence that Mo similarly stabilizes the dispersion of Pd in MgO-supported samples (20). A rough model of Pd–Mo clusters on the MgO surface was postulated (20), whereby the oxophilic Mo cations bond to support oxygen atoms and to Pd and thereby help to maintain the Pd dispersion. EXAFS data (20) showed that the Mo was concentrated at the metal–support interface, but there was also evidence of Pd–O interactions.

We suggest a similar structure for the Pt–W clusters on MgO. Such a structure could form from adsorbed $\{Pt[W(CO)_3(C_5H_5)]_2(PhCN)_2\}$. The results are consistent with the postulate that W–Pt–W units in this precursor were largely retained following removal of the ligands by H_2 treatment. Upon ligand removal, some of the metal centers likely became coordinatively unsaturated, so that there was a free energy driving force for formation of metal–metal bonds and migration and organization of the metal atoms into clusters on the surface, with the oxophilic W cations being preferentially anchored to the surface oxygen. Thus the Pt clusters are inferred to be stabilized in a high dispersion by their interactions with W cations, which are held in place by bonds to the surface oxygen atoms.

Catalytic properties. Benzene and toluene hydrogenation are structure-insensitive reactions, taking place with roughly the same turnover frequencies on the surfaces of metal particles of different sizes (60). However, the rate of toluene hydrogenation becomes size dependent as iridium clusters become as small as 4- or 6-atom clusters (61). The data of Table 5 show that the turnover frequency characteristic of the sample made from $[PtCl_2(PhCN)_2] + [Mo(CO)_6]$ and reduced at 400°C was about the same as that of Pt/MgO, and that characteristic of the sample made from $[PtCl_2(PhCN)_2] + [W(CO)_6]$, (Pt + W)/MgO, is somewhat lower than that of Pt/MgO. The structural data for the W- and Mo-containing samples, taken together, show that coimpregnation of separate complexes of Pt and an oxophilic metal leads to largely segregated metals. The catalytic data confirm this conclusion and show that there were at most small effects of Mo and W on the catalytic properties of supported Pt for toluene hydrogenation.

In contrast, the turnover frequencies characteristic of the samples made from the bimetallic precursors are more than an order of magnitude less than those characteristic of the samples containing segregated Pt. The data are in a good agreement with literature data (11) showing a decrease in the activity of Pt for hydrocarbon conversion when the Pt atoms are in proximity to cations of oxophilic metals. The catalytic data (Table 5) show that the apparent activation energy for toluene hydrogenation was 11–13 kcal/mol for all the samples, independent of catalyst composition and the nature of oxophilic metal. These values are about the same as those reported for toluene hydrogenation catalyzed by Pt (45) and close to the values for benzene hydrogenation on Pt (44). Thus, we suggest that the mechanism of toluene hydrogenation may be the same for the family of samples reported here as for those reported by Lin and Vannice (62), with the rate-determining step being the addition of the first hydrogen atom to the aromatic ring (62). The data summarized here show that strong Pt–W or Pt–Mo interactions are associated with a low activity relative to those observed for catalysts containing the same metals but lacking the strong bimetallic interactions. The samples with the relatively low activities are those characterized by the small Pt clusters as well as by relatively low hydrogen chemisorption on Pt; these effects are attributed, at least in part, to the Pt–W (or Pt–Mo) interactions in the samples. In addition, the low concentrations of hydrogen on the Pt surface during catalysis (expected on the basis of the chemisorption data) could also cause the catalytic reaction rate to be less than on Pt lacking the bimetallic interactions.

It is not yet possible to resolve which of these effects might be most important in decreasing the rates of toluene hydrogenation on the samples prepared from bimetallic clusters. Nonetheless, there is little doubt that Pt–W (or Pt–Mo) interactions lead to changes in the electronic and chemisorptive properties of Pt, and thereby its catalytic properties. The role of the W (or Mo) is thus comparable to that of a support, even though the W (or Mo) was present in only a small amount, localized near the Pt.

ACKNOWLEDGMENTS

We thank Professor D. C. Koningsberger of the University of Utrecht for helpful comments about the EXAFS analysis. This research was supported by Ford Motor Co. and the National Science Foundation (CTS-9529455). The equipment for adsorption measurements was purchased with support from a grant from the U.S. Department of Energy University Research Instrumentation Program. The EXAFS data were analyzed with the XDAP software (Vaarkamp, M., Linders, J. C., and Koningsberger, D. C., *Physica B* **209**, 159 (1995)). We acknowledge the support of the U.S. Department of Energy, Division of Materials Sciences, under Contract DE-FG05-89ER45384, for its role in the operation and development of beam line X-11A at the National Synchrotron Light Source. The NSLS is supported by the Department of Energy, Division

of Materials Sciences and Division of Chemical Sciences, under Contract DE-AC02-76CH00016. We are grateful to the staff of beam line X-11A for their assistance.

REFERENCES

1. Antos, G. A., Aitani, A. M., and Parera, J. M. (Eds.), "Catalytic Naphtha Reforming." Dekker, New York, 1995.
2. Shelef, M., *Catal. Rev.—Sci. Eng.* **11**, 1 (1975).
3. Taylor, K. C., *in* "Catalysis Science and Technology" (J. R. Anderson and M. Boudart, Eds.), p. 119. Springer, Berlin, 1984.
4. Wei, J., *Adv. Catal.* **11**, 57 (1975).
5. Kummer, J. T., *J. Phys. Chem.* **90**, 4747 (1986).
6. Pfefferle, L. D., and Pfefferle, W. C., *Catal. Rev.—Sci. Eng.* **29**, 219 (1987).
7. Taylor, K. C., *Catal. Rev.—Sci. Eng.* **35**, 457 (1993).
8. Shelef, M., and Graham, G. W., *Catal. Rev.—Sci. Eng.* **36**, 433 (1994).
9. Ismagilov, Z. R., Kerzhentsev, M. A., and Susharina, T. L., *Russ. Chem. Rev.* **59**, 973 (1990).
10. Sinfelt, J. H., "Bimetallic Catalysts: Discoveries, Concepts, and Applications." Wiley, New York, 1983.
11. Yermakov, Yu. I., Kuznetsov, B. N., and Zakharov, V. A., "Catalysis by Supported Complexes." Elsevier, Amsterdam, 1981.
12. Levin, M. E., Salmeron, M., Bell, A. T., and Somorjai, G. A., *J. Catal.* **106**, 401 (1987).
13. Basset, J.-M., Candy, J. P., Choplin, A., Nedez, C., Quignard, F., Santini, C. C., and Theolier, A., *Mat. Chem. Phys.* **29**, 5 (1991).
14. Braunstein, P., and Rose, J., *in* "Stereochemistry of Organometallic and Inorganic Compounds" (I. Bernal, Ed.), p. 3. Elsevier, Amsterdam, 1988.
15. Braunstein, P., *Mater. Chem. Phys.* **29**, 33 (1991).
16. Fung, A. S., McDevitt, M. R., Tooley, P. A., Kelley, M. J., Koningsberger, D. C., and Gates, B. C., *J. Catal.* **140**, 190 (1993).
17. Trunschke, A., Ewald, H., Miessner, H., Fukuoka, A., Ichikawa, M., and Böttcher, H.-C., *Mater. Chem. Phys.* **29**, 503 (1991).
18. Te, M., Lowenthal, E. E., and Foley, H. C., *J. Catal.* **146**, 591 (1994).
19. Choplin, A., Huang, L., Theolier, A., Gallezot, P., Basset, J.-M., Siriwardane, U., Shore, S. G., and Mathieu, R., *J. Am. Chem. Soc.* **108**, 4224 (1986).
20. Kawi, S., Alexeev, O., Shelef, M., and Gates, B. C., *J. Phys. Chem.* **99**, 6926 (1995).
21. Alexeev, O., Kawi, S., Shelef, M., and Gates, B. C., *J. Phys. Chem.* **100**, 253 (1996).
22. Lamb, H. H., Gates, B. C., and Knözinger, H., *Angew. Chem. Int. Ed. Engl.* **27**, 1127 (1988).
23. Bender, R., Braunstein, P., Jud, J.-M., and Dusausoy, Y., *Inorg. Chem.* **23**, 4489 (1984).
24. Braunstein, P., Bender, R., and Jud, J.-M., *Inorg. Synth.* **26**, 341 (1989).
25. Zaikovskii V. I., Ryndin, Yu. A., Kovalchuk, V. I., Plyasova, L. M., Kuznetsov, B. N., and Yermakov, Yu. I., *Kinet. Katal.* **22**, 443 (1981).
26. Rehr, J. J., Mustre de Leon, J., Zabinsky, S. I., and Albers, R. C., *J. Am. Chem. Soc.* **113**, 5135 (1991).
27. Kirlin, P. S., van Zon, F. B. M., Koningsberger, D. C., and Gates, B. C., *J. Phys. Chem.* **94**, 8439 (1990).
28. van Zon, J. B. A. D., Koningsberger, D. C., van't Blik, H. F. J., and Sayers, D. E., *J. Chem. Phys.* **82**, 5742 (1985).
29. Koningsberger, D. C., and Prins, R. (Eds.), "X-Ray Absorption: Principles, Applications, Techniques of EXAFS, SEXAFS and XANES." Wiley, New York, 1988.
30. Koningsberger, D. C., *in* "Synchrotron Techniques in Interfacial Electrochemistry" (C. A. Melendres and A. Tadjeddine, Eds.), p. 181. Kluwer, Dordrecht, 1994.
31. Malinowski, S. T., Szczepanska, S., and Sloczynski, J., *J. Catal.* **7**, 67 (1967).
32. Davydov, A. A., "Infrared Spectroscopy of Adsorbed Species on the Surfaces of Transition Metal Oxides." Wiley, Chichester, 1990.
33. Fritz, H. P., *Adv. Organomet. Chem.* **1**, 239 (1964).
34. Nakamoto, K., "Infrared and Raman Spectra of Inorganic and Coordination Compounds." Wiley, New York, 1970.
35. Little, L. H., "Infrared Spectra of Adsorbed Species." Academic Press, London, 1966.
36. Primet, M., Elazhar, M., Frety, R., and Guenin, M., *Appl. Catal.* **59**, 153 (1990).
37. Hayden, B. E., and Bradshaw, A. M., *Surf. Sci.* **125**, 787 (1983).
38. Barth, R., and Ramachandran, A., *J. Catal.* **125**, 467 (1990).
39. Tobin, R. G., Phelps, R. B., and Richards, P. L., *Surf. Sci.* **183**, 427 (1987).
40. Wong, Y.-T., and Hoffmann, R., *J. Phys. Chem.* **95**, 859 (1991).
41. Gebhard, S. C., Windham, R. G., and Keol, B. E., *J. Phys. Chem.* **94**, 6831 (1990).
42. Balakrishnan, K., Sachdev, A., and Schwank, J., *J. Catal.* **121**, 441 (1990).
43. Primet, M., and Meriaudeau, P., *Appl. Catal.* **52**, 263 (1989).
44. Lin, D. S., and Vannice, M. A., *J. Catal.* **143**, 539 (1993).
45. Lin, D. S., and Vannice, M. A., *J. Catal.* **143**, 554 (1993).
46. Gates, B. C., and Lamb, H. H., *J. Mol. Catal.* **52**, 1 (1989).
47. Ichikawa, M., *in* "Tailored Metal Catalysts" (Y. Iwasawa, Ed.), p. 183. Reidel, Dordrecht, 1986.
48. Otten, M. M., and Lamb, H. H., *J. Am. Chem. Soc.* **116**, 1372 (1994).
49. Dufour, P., Houtman, C., Santini, C. C., Nedez, C., Basset, J.-M., Hsu, L. Y., and Shore, S. G., *J. Am. Chem. Soc.* **114**, 4248 (1992).
50. Purnell, S. K., Sanchez, K. M., Patrini, R., Chang, J.-R., and Gates, B. C., *J. Phys. Chem.* **98**, 1205 (1994).
51. Ryndin, Yu. A., Alekseev, O. S., Paukshtis, E. A., Kalinkin, A. V., and Kochubey, D. I., *Appl. Catal.* **63**, 51 (1990).
52. Guglielminotti, E., and Zecchina, A., *J. Mol. Catal.* **24**, 331 (1984).
53. Kampers, F. W. H., Engelen, C. W. R., van Hooff, J. H. C., and Koningsberger, D. C., *J. Phys. Chem.* **94**, 8574 (1990).
54. Anderson, J. R., "Structure of Metallic Catalysts." Academic Press, London, 1975.
55. Alekseev, O. S., and Ryndin, Yu. A., *Russ. Chem. Rev.* **61**, 417 (1992).
56. Blyholder, G., *J. Phys. Chem.* **68**, 2772 (1964).
57. Linsebigler, A., Lu, G., and Yates, J. T., Jr., *Surf. Sci.* **294**, 284 (1993).
58. Kudo, M., Garfunkel, E. L., and Somorjai, G. A., *J. Phys. Chem.* **89**, 3207 (1985).
59. Kiskinova, M., Pirug, G., and Bonzel, H. P., *Surf. Sci.* **133**, 321 (1983).
60. Boudart, M., and Djéga-Mariadassou, G., "Kinetics of Heterogeneous Catalytic Reactions." Princeton Univ. Press, Princeton, 1984.
61. Xu, Z., Xiao, F.-S., Purnell, S. K., Alexeev, O., Kawi, S., Deutsch, S. E., and Gates, B. C., *Nature (London)* **372**, 346 (1994).
62. Lin, D. S., and Vannice, M. A., *J. Catal.* **143**, 563 (1993).